Yukutake and Iio *Earth, Planets and Space* (2017) 69:68
DOI 10.1186/s40623-017-0650-2

Earth, Planets and Space

FULL PAPER

Open Access

Why do aftershocks occur? Relationship between mainshock rupture and aftershock sequence based on highly resolved hypocenter and focal mechanism distributions

Yohei Yukutake[1*] and Yoshihisa Iio[2]

Abstract

In order to clarify the origin of aftershocks, we precisely analyze the hypocenters and focal mechanisms of the aftershocks following the 2000 Western Tottori Earthquake, which occurred in the western part of Japan, using data from dense seismic observations. We investigate whether aftershocks occur on the mainshock fault plane on which coseismic slip occurred or they represent the rupture of fractures surrounding the mainshock fault plane. Based on the hypocenter distribution of the aftershocks, the subsurface fault structure of the mainshock is estimated using principal component analysis. As a result, we can obtain the detail fault structure composed of 8 best-fit planes. We demonstrate that the aftershocks around the mainshock fault are distributed within zones of 1.0–1.5 km in thicknesses, and their focal mechanisms are significantly diverse. This result suggests that most of the aftershocks represent the rupture of fractures surrounding the mainshock fault rather than the rerupture of the mainshock fault. The aftershocks have a much wider zone compared with the exhumed fault zone in field observations, suggesting that many aftershocks occur outside the fault damage zone. We find that most aftershocks except in and around the large-slip region are well explained by coseismic stress changes. These results suggest that the thickness of the aftershock distribution may be controlled by the stress changes caused by the heterogeneous slip distribution during the mainshock. The aftershock is also distributed within a much wider zone than the hypocenter distribution observed in swarm activity in the geothermal region, which is thought to be caused by the migration of hydrothermal fluid. This result implies a difference in generation processes: Stress changes due to the mainshock contribute primarily to the occurrence of aftershocks, whereas earthquake swarms in the geothermal region are caused by fluid migration within the localized zone.

Keywords: Aftershock, Fault plane of mainshock, Fault damage zone, Hypocenter distribution, Focal mechanism

Background

Understanding why aftershocks occur is one of the major unsolved problems in seismology, and several generation mechanisms of aftershocks have been proposed. For example, aftershocks have been thought to be reruptures of remnants on the fault surface that were not broken by the mainshock, to be generated by stress concentrations of the mainshock slip (e.g., Das and Henry 2003) and to be triggered by strength reductions due to high pore fluid pressure caused by the mainshock slip (e.g., Miller et al. 2004). Although all of these mechanisms have reasonable physical bases, which mechanism is actually at work has rarely been confirmed based on precise aftershock data.

The hypocenter distribution of aftershocks has been recognized to reflect the structure of the fault plane that was ruptured during the mainshock. Thus, a number of previous studies estimated the subsurface structure of the mainshock fault plane based on the aftershock distribution (e.g., Shibutani et al. 2005a; Kato 2005). On the other

*Correspondence: yukutake@onken.odawara.kanagawa.jp
[1] Hot Springs Research Institute of Kanagawa Prefectural Government, Odawara, Japan
Full list of author information is available at the end of the article

hand, field observation of an exhumed outcrop has demonstrated that a fault damage zone is developed around a fault core that is the localized slip zone and contains high-strain products, such as gouges, cataclasites, and ultracataclasites (Mitchell and Faulkner 2009). The fault damage zone has also been identified using geophysical data, such as seismic travel times or trapped waves (e.g., Cochran et al. 2009; Ben-Zion et al. 2003). We have not clarified what an aftershock distribution represents, specifically, whether aftershocks reflect the rerupture of the mainshock fault plane or the rupture of the damage zone surrounding the mainshock fault plane or whether aftershocks occur outside the damage zone. This is important to clarifying the generation mechanism of aftershocks.

Liu et al. (2003) investigated the hypocenter catalog of the aftershock sequence following the 1993 Mw 7.3 Landers earthquake and concluded that only 5% of aftershocks occurred on the mainshock fault plane. However, since the location errors of the aftershock hypocenters in their study were up to 1 km, discussion based on more precisely determined hypocenters is essential. Moreover, a focal mechanism solution of aftershocks provides additional information associated with the orientation of the fault plane. We analyzed the aftershock sequence of the 2000 Western Tottori Earthquake that occurred in an intraplate region. A dense seismic observation network composed of 48 temporary stations was installed immediately after the mainshock. The high-quality observation data provide an excellent opportunity to clarify the above issue.

In the present study, we estimate the hypocenter locations and focal mechanisms of the aftershocks of the 2000 Western Tottori Earthquake using dense seismic observations. We examine the fault model of the mainshock based on precisely determined hypocenter locations. Moreover, we discuss the relationship between the subsurface fault structure of the mainshock and the aftershock distribution.

Overview of the 2000 Western Tottori Earthquake

The 2000 Western Tottori Earthquake occurred on October 6, 2000, in the western part of Tottori Prefecture in southwestern Honshu, Japan (Fig. 1). The moment magnitude was determined to be 6.6 (Fukuyama et al. 2003). Iwata and Sekiguchi (2002) estimated the slip distribution of the mainshock using near-field strong motion waveforms and geodetic data and found that coseismic slip occurred on the southern part of the aftershock region, while there was little moment release on the northern part of the aftershock region (Fig. 2b). Sagiya et al. (2002) also estimated the slip distribution using global navigation satellite system (GNSS) data and reported that most of the seismic moment during the mainshock was released on the fault plane in the southern part of the aftershock region, whereas afterslip occurred on the fault planes in the northern part of the aftershock region. Fukuyama et al. (2003) estimated the fault model of the Western Tottori Earthquake using the detailed distribution of the aftershock hypocenters and their centroid moment tensor (CMT) solutions. However, they used only seismic data obtained by permanent stations in and around the aftershock region with a station interval of approximately 20 km. Therefore, the locations of the aftershock hypocenters in their study contain large uncertainty.

Data and methods

Determination of hypocenters and focal mechanisms

A total of 48 temporary stations were installed in and around the aftershock region during the period from 13 October to early December 2000 (Shibutani et al. 2005b). Together with data from seven permanent stations, the dense seismic observation network was developed with an average station spacing of 4–5 km near the center of the aftershock region (Fig. 1). We manually picked the arrival time of the P- and S-waves and the polarities of the P-waves for 4770 local events that occurred during the period from October 15, to November 31, 2000. The local magnitudes of these events ranged from 0.4 to 3.9.

In order to obtain the initial hypocenter locations, we selected 4190 events for which the P- or S- wave arrival times were obtained at eight or more stations. The initial hypocenter locations were obtained by applying the one-dimensional velocity model and the station corrections estimated by Shibutani et al. (2005b) to the method of hypocenter determination developed by Kawanishi et al. (2009), which is a modified version of the Hypomh program code (Hirata and Matsu'ura 1987).

The double-difference relocation (DD) method (Waldhauser and Ellsworth 2000) was applied to the initial hypocenter data. The differential arrival time data for the manually picked P- and S-waves consisted of 597,744 and 270,359 pairs, respectively. We also used the differential arrival times obtained by cross-correlation analysis. The correlation analysis was conducted using a velocity waveform with a time window of 0.5 s, including the manually picked arrival times, applying a band-pass filter between 3 and 20 Hz. We used only the differential arrival time data with normalized cross-correlation coefficients greater than or equal to 0.8. Using this threshold, we obtained cross-correlation data consisting of 307,447 pairs for the P-wave and 177,677 pairs for the S-wave. After application of the DD method, 4089 events were successfully relocated (Fig. 2). The root-mean-square (RMS) of the double-difference time residual decreased from 95 to 30 ms for the manually

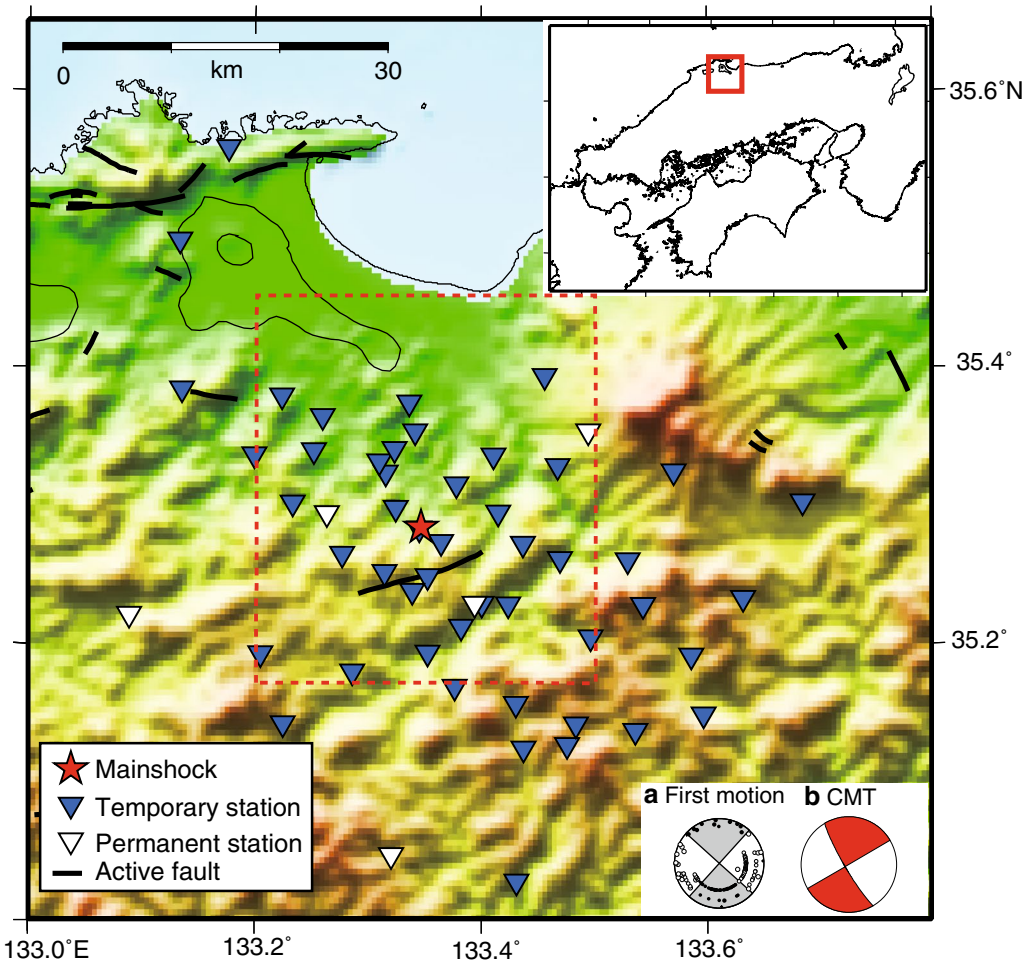

Fig. 1 *Map* showing the spatial distribution of seismic stations (*blue*: temporary stations, *white*: permanent stations). The *red star* indicates the starting point of rupture during the 2000 Western Tottori Earthquake. The area indicated by the *broken red rectangle* corresponds to the area appearing in Figs. 2, 3, and 4. In the *inset map*, the target region is shown with respect to the western part of the Japanese Islands. The *thick black lines* indicate the surface traces of active faults compiled by the Research Group for Active Faults in Japan (1991). The focal mechanism of the mainshock determined using the P-wave polarities (Ohmi et al. 2002) and CMT inversion (Fukuyama et al. 2003) are shown in (*a*) and (*b*), respectively

picked data and decreased from 61 to 7 ms for the cross-correlation data.

In order to assess the uncertainty in the relative hypocenter locations by the DD method, we applied a bootstrap resampling method (Shearer 1997; Waldhauser and Ellsworth 2000) for the relocated events. As a result, two standard deviations (2σ) of the relative location errors for the events relocated using both the manually picked and cross-correlation data are 26 m in the N–S direction, 30 m in the E–W direction, and 65 m in the depth direction. These events account for 76% of all relocated events. For the remaining events relocated using only the manually picked data, 2σ of the relative location errors are 50 m in the N–S direction, 81 m in the E–W direction, and 125 m in the depth direction.

We estimated the focal mechanism using the absolute amplitude of the P- and SH-waves, as well as the P-wave polarities, following the method proposed by Imanishi et al. (2006). The spectral level and corner frequency were determined by fitting ω^2 model with an attenuation correction following the method of Ide (2003). The spectral levels in the low-frequency range were used as the observed amplitudes. As indicated by Imanishi et al. (2004), the spectral levels for the low-frequency range can be stably estimated, while the corner frequency and the attenuation correction are not well resolved from each other in the spectral fitting. The best-fit solution of the focal mechanism was determined by minimizing the residual between the observed and theoretical amplitudes, with a grid

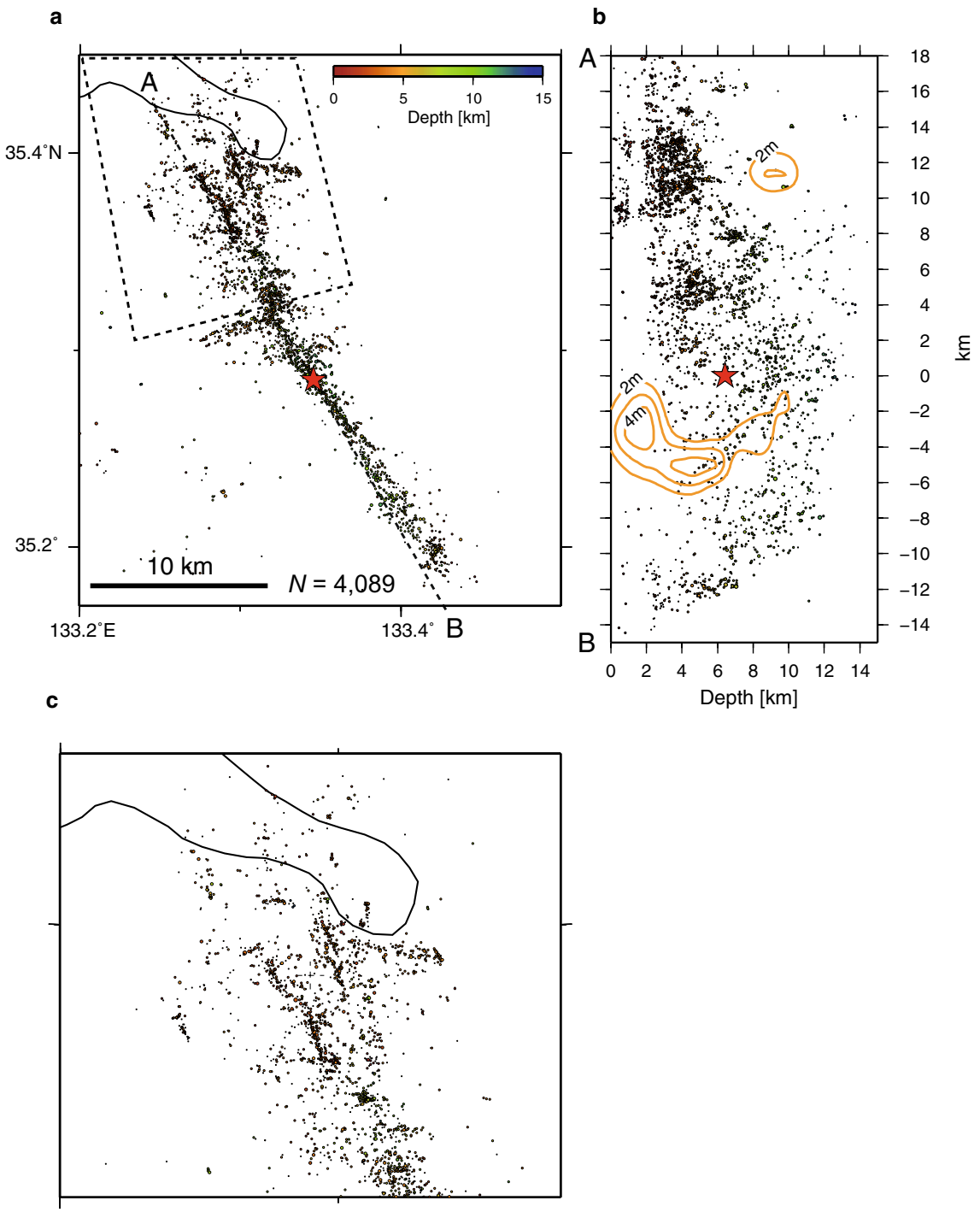

Fig. 2 Hypocenter distribution of the aftershocks determined by the DD method. The depth of the hypocenter is indicated by the *color scale*. **a** Epicentral distribution, **b** depth distribution projected onto *line A–B* in (**a**), and (**c**) magnified image of the northern part of the aftershock region. Earthquakes within a distance of 6 km from the *line* are projected in (**b**). The *orange* contours projected on *line A–B* in (**b**) indicate areas of large slip exceeding a dislocation of 2.0 m as estimated by Iwata and Sekiguchi (2002). The northern part of the aftershock region is indicated by the area enclosed by the *broken line* in (**a**)

search method at a 5° interval in the strike, dip, and rake angles. In order to calculate the azimuth and take-off angles, we used the relocated hypocenters by the DD method and the one-dimensional velocity models obtained by Shibutani et al. (2005b). We applied the amplitude station corrections estimated from the average ratio of the observed and theoretical amplitudes. Following the method proposed by Yukutake et al. (2008), we estimated the uncertainty in the focal mechanism solutions using Kagan's rotation angle (Kagan 1991). We could determine focal mechanisms of 3269 events (Fig. 3) with the uncertainty of the solution less than 15°. These events account for 80% of the 4089 relocated events.

Estimation of subsurface fault structure

Since surface faulting was not emerged above the aftershock region of the 2000 Western Tottori Earthquake (Ueta et al. 2002), we estimated the subsurface structure of the mainshock fault plane based on the relocated hypocenter distribution. We applied principal component analysis (PCA) (Shearer et al. 2003) to the hypocenter data. In this analysis, the eigenvalues and eigenvectors of the covariance matrices in the x (E–W), y (N–S), and z (depth) coordinates of the hypocenter locations with respect to their mean locations were calculated. Eigenvector U_1 corresponding to the largest eigenvalue, λ_1, defines the longest axis of an ellipsoid for the hypocenter distribution. The planarity of the hypocenter distribution

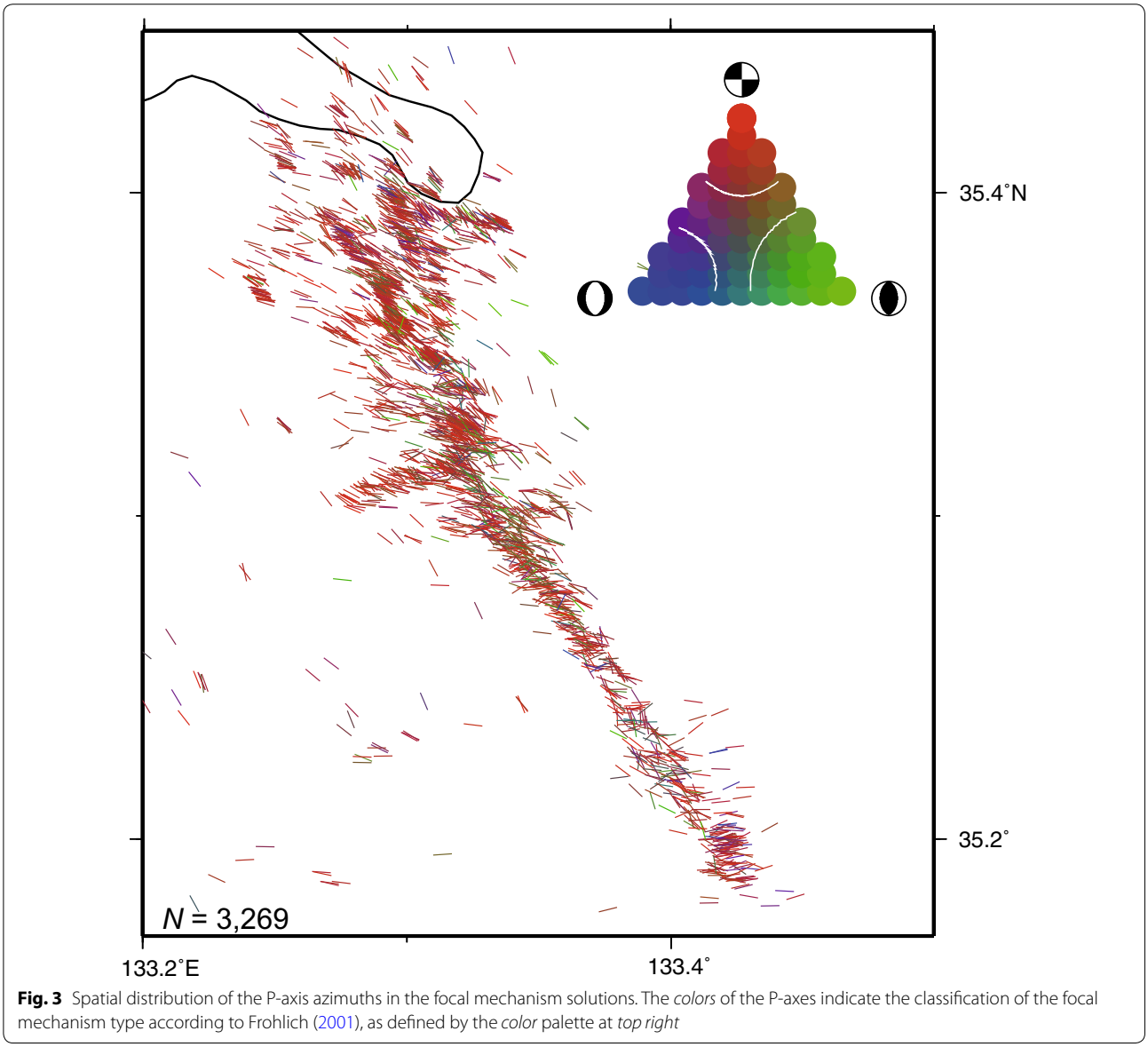

Fig. 3 Spatial distribution of the P-axis azimuths in the focal mechanism solutions. The *colors* of the P-axes indicate the classification of the focal mechanism type according to Frohlich (2001), as defined by the *color* palette at *top right*

was characterized by the ratio of the middle eigenvalue to the smallest eigenvalue (λ_2/λ_3). We defined a hypocenter distribution with a planarity greater than or equal to 8 as a planar distribution, following the criterion in Shearer et al. (2003). For the planar distribution, the strike and dip angles of the best-fit plane were calculated using eigenvectors. We also estimated the standard deviation (σ) of the best-fit plane orientation using a bootstrap resampling method.

The selection of events for PCA was followed by these steps. First, we divided the aftershock region into the northern and southern parts (Fig. 2a) based on the characteristics of hypocenter distribution. Then, we conducted PCA for the hypocenter data in each part. If the result meets the following three conditions, we estimated the best-fit fault plane for the region: (1) Planarity of the hypocenter distribution is greater than or equal to 8.0, (2) standard deviation of the plane orientation is less than or equal to 2.0°, (3) number of event in the region is greater than or equal to 20. If the result did not meet the first or second conditions, we divided the region into smaller parts based on the hypocenter distribution and conducted PCA for each small region again to obtain as many fault planes as possible. This procedure was repeated 4 times, assuming that the subsurface fault structure is simple. The spatial division for event selection in each step and the results of PCA are shown in Additional file 1. As a result, we obtained 8 best-fit fault planes that represent the planar distribution with a standard deviation of the plane orientation of less than 2° (Table 1; Fig. 4). We assumed that the best-fit planes define the position and orientation of the subsurface fault structure.

Figure 5 shows an example of the hypocenter distribution around the best-fit plane in the southern and northern parts of the aftershock region. The width and length of the best-fit plane were estimated from an edge of the hypocenter distribution projected onto the best-fit plane (middle diagram in Fig. 5). The event location projected onto the shortest axis (x-axis of right-hand diagram in Fig. 5) was used to calculate the thickness of the hypocenter distribution. We defined the thickness of the aftershock distribution (A_t) as the range on the shortest axis in which 90% of the aftershocks are contained. In order to evaluate the variety of focal mechanisms, we define a reference focal mechanism based on the orientation of best-fit plane. The strike and dip angles of the reference focal mechanism were assumed to be those of the best-fit plane (Table 1). The rake angle of the reference focal mechanism was assumed to be parallel to the resolved shear stress direction on the best-fit plane under the stress field reported by Yukutake et al. (2007), in which the stress field around the mainshock fault was estimated using a stress inversion method and focal mechanism data of the aftershocks.

Results

In the southern parts of the aftershock region, the aftershocks are distributed primarily along a line in the NNW–SSE direction (Fig. 2a). The best-fit planes in this region (Faults 1 and 2) are consistent with the orientation of one of the nodal planes in the CMT solution of the mainshock (e.g., Fukuyama et al. 2003). A large slip of more than 2 m occurred on Fault 1 during the mainshock (Fig. 2b) (Iwata and Sekiguchi 2002). On the other hand, in the northern part of the aftershock region, a complicated spatial distribution of the aftershocks was estimated. The hypocenter distribution of the aftershocks suggests the existence of a conjugate fault system and is divided into several small clusters. The complicated structures of the best-fit plane were estimated (Faults 5 through 8).

Figure 6 shows the frequency distribution of the distance from the best-fit plane to each aftershock location. The aftershocks were concentrated on the best-fit plane, and the concentration decreased with the distance from the best-fit plane. Figure 7 shows a histogram of A_t around the 8 best-fit planes. The aftershocks around Faults 1 through 4 are distributed with zones of 1.0–1.5 km in thicknesses.

Most of the focal mechanisms are of the strike-slip type. The P-axes of focal mechanisms are oriented primarily in the directions ranging from E–W to NW–SE (Fig. 3). These features of the focal mechanisms are consistent with those reported in previous studies (e.g., Yukutake et al. 2007). We also evaluated the variety of the focal mechanisms based on the Kagan angle (1991) from the reference focal mechanism. The focal mechanisms of the aftershocks have wide Kagan angle ranges, exceeding 100° (Fig. 6). A total of 90% of the focal mechanisms have a Kagan angle of greater than 15°, which corresponds to the upper limit of the uncertainty in the focal mechanism solutions. These results imply that the aftershocks do not occur on a simple plane. The peak of the frequency distribution was observed around Kagan angles of 20°–30°. Figure 8a shows the relationship between the hypocenter distance from Fault 1 or 2 and the Kagan angle from the reference focal mechanism. The focal mechanisms having Kagan angles of around 20°–30° were concentrated near the best-fit planes. Figure 8b, c shows the azimuth of one of the nodal planes close to the strike of each best-fit plane for strike-slip events, the plunges of the P- and T-axes of which are less than or equal to 30°, respectively. Most nodal planes of these focal mechanisms are oriented obliquely with respect to each best-fit plane rather than coincident with it.

Table 1 Parameters of the best-fit fault planes

Fault no.	Lon (°)	Lat (°)	Depth (km)	Strike (°)	Dip (°)	Rake (°)	Length (km)	Width (km)	Thickness (km)	Planarity	Sd strike (°)	Sd dip (°)
1	133.4023	35.2187	6.8	150	83	3	9.3	10.5	1.48	15.9	0.7	0.8
2	133.3533	35.2782	8.1	144	90	0	5.0	11.1	1.28	11.1	1.0	0.7
3	133.3377	35.2998	6.7	77	88	180	5.1	10.9	1.10	9.4	1.4	0.5
4	133.3130	35.3158	5.6	251	89	180	6.6	11.5	1.16	15.4	0.8	0.6
5	133.3109	35.3361	5.7	257	88	180	5.4	7.6	0.98	12.9	1.2	0.7
6	133.2797	35.3840	3.3	317	87	3	3.7	4.7	1.02	8.1	1.8	1.1
7	133.3021	35.3845	4.0	161	88	0	5.6	7.9	1.34	8.9	1.0	1.3
8	133.3259	35.3915	4.3	93	82	174	2.6	3.1	0.46	8.6	1.4	1.9

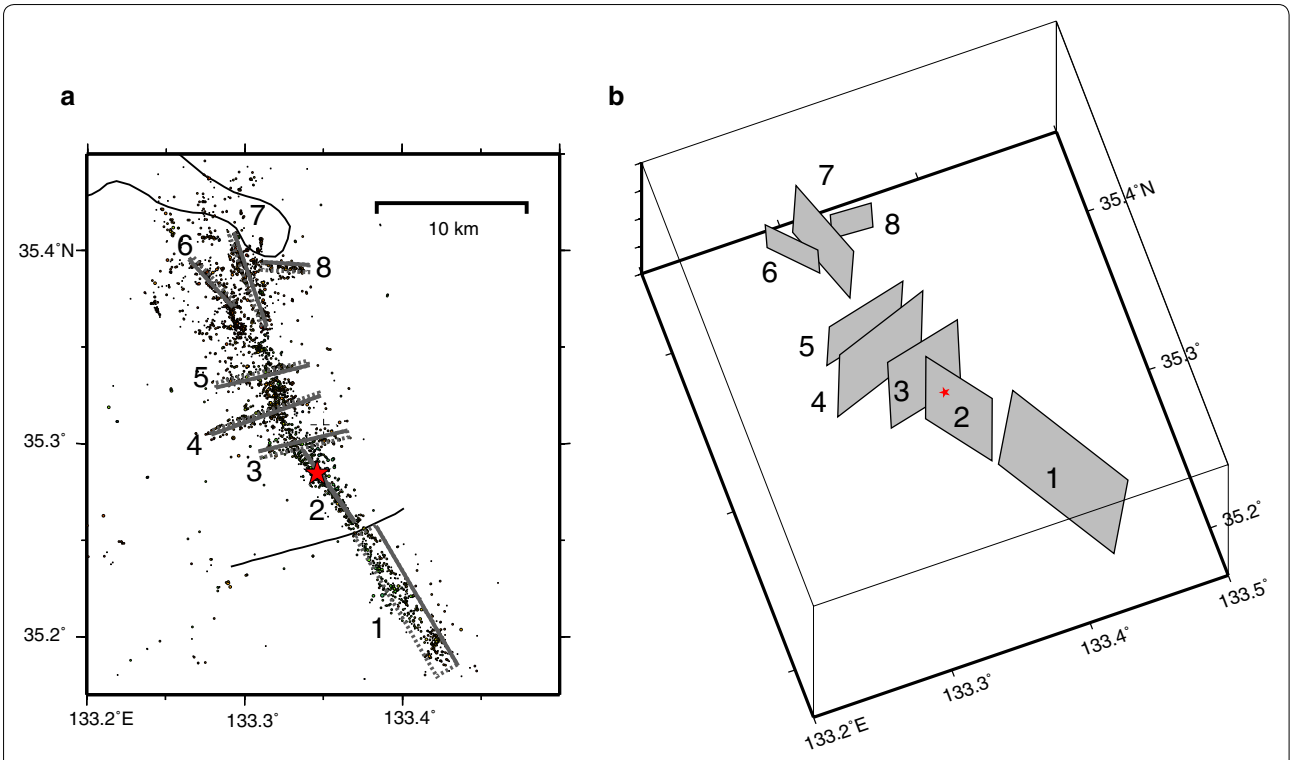

Fig. 4 Best-fit fault planes of the 2000 Western Tottori Earthquake by PCA. **a** *Map* view with the relocated aftershock hypocenters. **b** Perspective view of fault orientations. *Numbers* correspond to the index numbers of faults listed in Table 1

Discussion

Difference in fault geometries between the northern and southern parts of the aftershock region

The general features of the fault model obtained in the present study are consistent with those reported by Fukuyama et al. (2003). However, the locations of the best-fit planes in the northern part of the aftershock region were estimated at shallower depths compared with their fault model. This difference results from the uncertainty of the hypocenter depth in their study due to a lack of seismic stations above the northern part of the aftershock region. According to the result of Sagiya et al. (2002), the seismic moment during the mainshock was mainly released in the southern part of the aftershock region, whereas afterslip occurred in the northern part of the aftershock region. Fukuyama et al. (2003) reported that the aftershocks immediately following the mainshock occurred only in the southern part of the aftershock region. Based on these results, seismic slip during the mainshock is inferred to have occurred on Faults 1 through 4. Therefore, these best-fit planes of Faults 1 through 4 can be defined as the "mainshock fault." On the other hand, the aftershocks around Faults 5 through 8 may be mainly related to the afterslip.

The conjugate fault plane of Fault 4 was estimated at the northern edge of the mainshock fault. Shibutani et al. (2005b) estimated the velocity boundary around Fault 4. A high-velocity structure corresponding to plutonic and metamorphic rocks was estimated along the mainshock fault (in the southern part of aftershock region), whereas the northern part of the aftershock region was composed primarily of non-alkali volcanic and pyroclastic rocks of the early to middle Miocene, which are characteristic of a low-velocity zone. The characteristics of fault structures appear to differ at this velocity boundary. A complicated fault system developed on the northern side, whereas a larger fault structure on the order of 10 km in length existed on the southern side (Fig. 4). The dynamic rupture process of the 2000 Western Tottori Earthquake was probably controlled by these pre-existing fault structures around the source region.

Is the thickness of the aftershock distribution real?

The aftershocks are distributed within approximately 1.0–1.5 km in thicknesses from the mainshock fault plane (Figs. 6, 7). Location errors of hypocenters in the horizontal direction strongly affect A_t for a nearly vertical dipping fault plane, as observed in the study region.

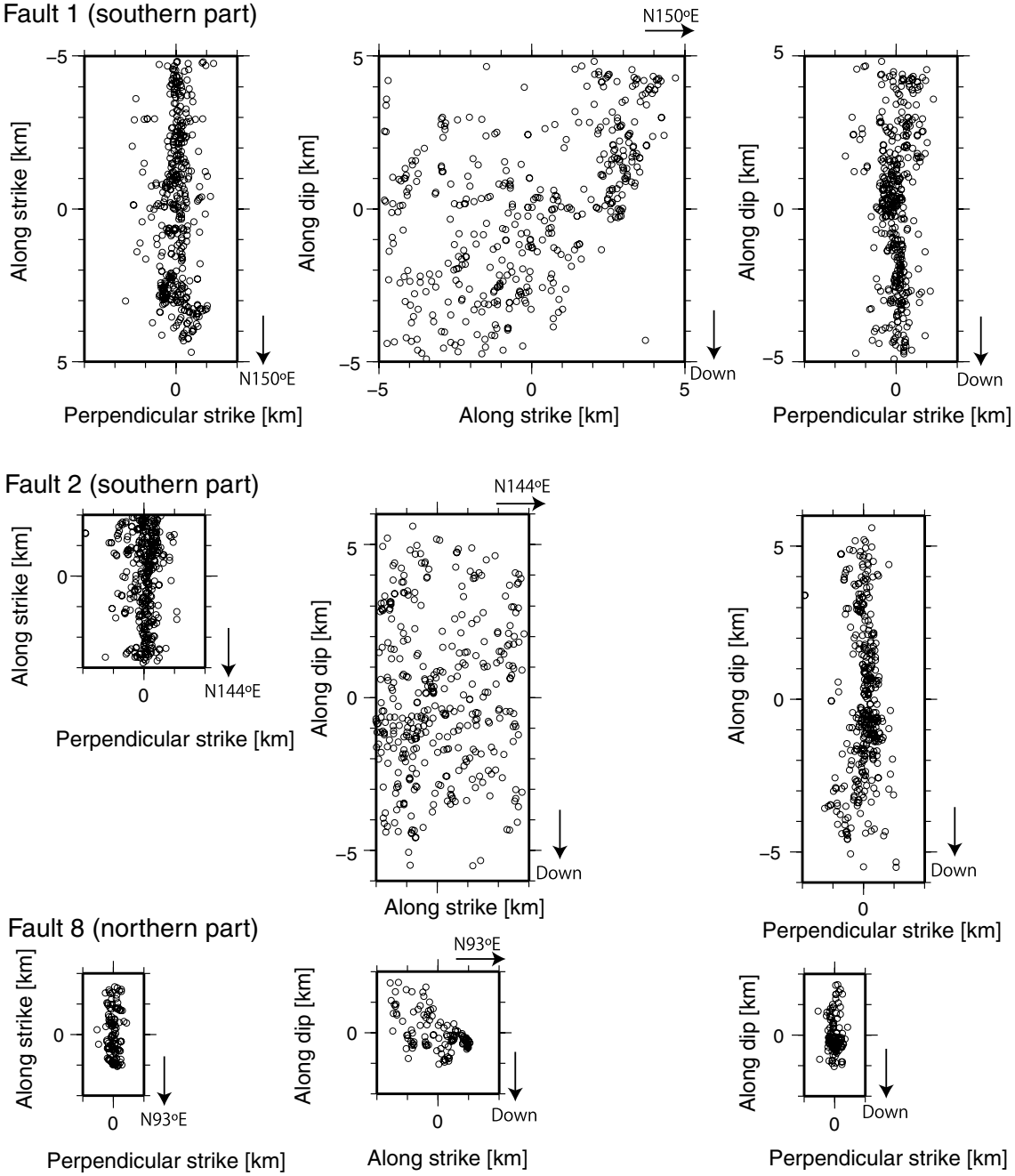

Fig. 5 Hypocenter distribution around the best-fit planes. (*Left*) Hypocenter distribution along the strike of the best-fit plane. The *vertical* and *horizontal axes* indicate, respectively, the directions along and normal to the best-fit plane. (*Middle*) and (*right*) Hypocenter distributions projected onto and perpendicular to the best-fit fault plane, respectively. (*Top*) Hypocenter distribution around Fault 1 (*middle*) that around Fault 2 and (*bottom*) that around Fault 8 in Fig. 4

However, the estimated thickness cannot be explained by the location errors of the hypocenter in the horizontal direction that are less than 30 m for differential arrival time data obtained by both catalog and cross-correlation analysis. There is also a possibility that the wide aftershock distribution around the mainshock fault results from a local irregularity in the mainshock fault geometry. In order to exclude this possibility, we conducted PCA for the hypocenters around Faults 1 and 2, dividing the area around the best-fit planes into 15

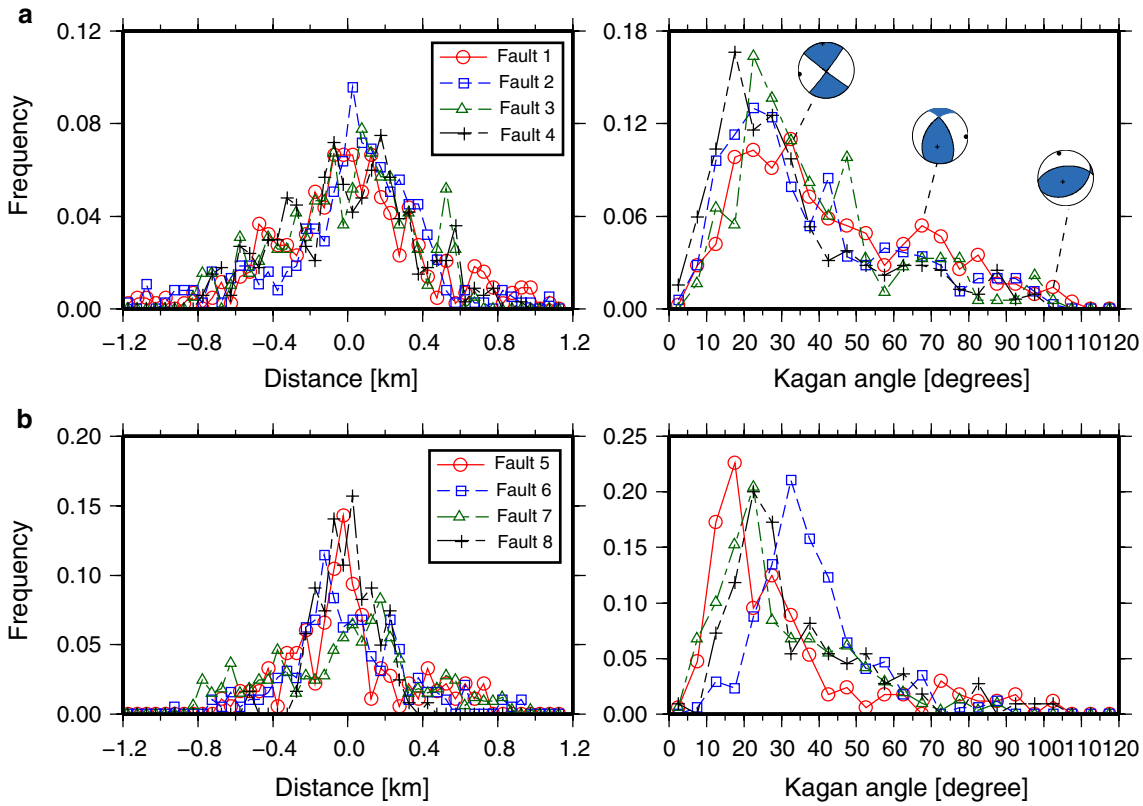

Fig. 6 Histograms showing the distance from the best-fit fault planes and the Kagan angles. (*Left*) The distance from the best-fit fault plane to each location of an aftershock. (*Right*) The Kagan angles from the reference focal mechanism. The *Y*-axis is normalized by the total number of events. **a** Faults 1 through 4, **b** Faults 5 through 8. Some examples of focal mechanisms around Fault 1 at the Kagan angle are also shown in (**a**)

small regions. The length of the hypocenter distribution is 2–3 km in the middle and longest axes. We analyzed only regions containing at least 20 earthquake hypocenters. As a result, we obtained A_t for 12 small regions ranging from 0.3 to 1.4 km (Fig. 7b). For seven small clusters, the planarity of the hypocenter distribution was less than eight. This means that A_t is close to the length of the middle axis for the seismicity (2–3 km). These results imply that A_t is not attributed to geometric heterogeneity of the mainshock fault. Validity of A_t can be also confirmed by using the observed differential arrival times for the small earthquake cluster (Additional file 2).

Estimation of aftershocks that occurred on the mainshock fault plane

Assuming the mainshock fault surface to be smooth and to coincide with the best-fit plane, the percentage of aftershocks occurring on the rupture surface of the mainshock fault can be estimated. Estimation was performed using earthquakes for which the hypocenters and focal mechanisms were obtained, which account for 96% of the relocated hypocenters around the regions of Faults 1 through 4. Considering the error of the hypocenter location and focal mechanism, we defined the aftershocks that occurred within ±30 m from the best-fit plane and have a Kagan angle of less than or equal to 15° as candidates for rerupture of the mainshock fault. As a result, only 1% of the aftershocks around Faults 1 through 4 were defined as rerupture of the mainshock fault. If we eased the condition for candidates to aftershocks that occurred within ±60 m from the best-fit plane and Kagan angles of less than or equal to 30°, then 7% of the aftershocks around Faults 1 through 4 were defined as rerupture of the mainshock fault. The result is consistent with the estimation by Liu et al. (2003).

Relationship between fault length and thickness of the aftershock distribution

Figure 9 shows the relationship between lengths of the best-fit plane (L) and A_t. The figure also shows the relationship between L and the damage zone thickness of a natural fault zone (P) in an outcrop (Vermilye and Scholz 1998). The aftershocks were distributed within a much wider zone than the fault damage zone at the same L.

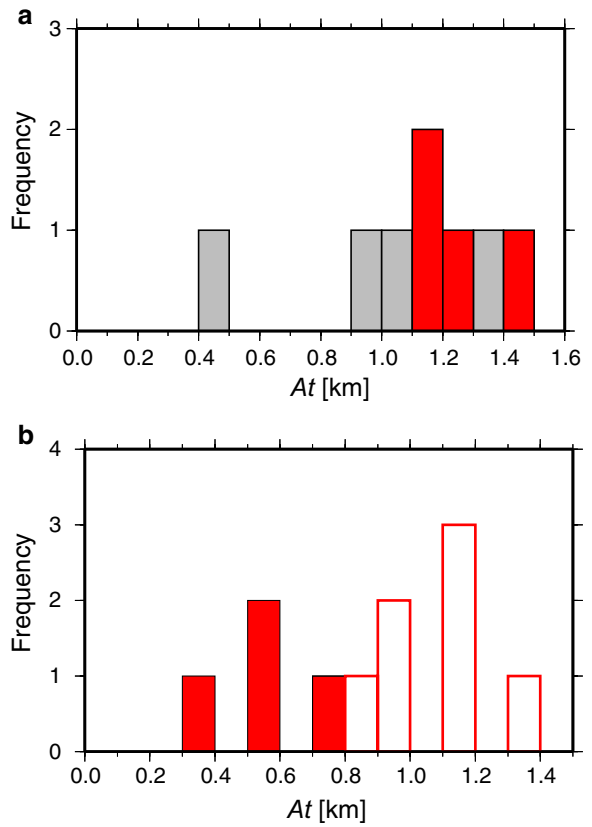

Fig. 7 Histograms showing A_t. **a** *Red* and *gray bins* correspond to A_t around the mainshock fault (Faults 1 through 4) and the best-fit planes in the northern part of the aftershock region (Faults 5 through 8), respectively. **b** *Each bin* shows A_t around Faults 1 and 2 estimated using a smaller region for event selection. The *solid* and *open bins* indicate, respectively, A_t with a planarity greater than or equal to 8 and A_t with a planarity less than 8

Using a seismic tomography with a spatial resolution of 2 km, Shibutani et al. (2005b) showed that the crustal structure along the mainshock fault of the 2000 Western Tottori Earthquake was characterized by high velocity and suggested that a wide kilometer-order damage zone did not develop because the mainshock fault was an immature young active fault. These results suggest that numerous aftershocks occurred outside the fault damage zone.

Are aftershocks triggered by coseismic stress changes?

Since A_t is likely to be not controlled by the thickness of fault damage zone, the coseismic stress changes by the mainshock are suggested as one of the plausible factors for affecting A_t. Nodal planes of the focal mechanisms oblique to the mainshock fault plane (Fig. 8) may reflect the contribution of stress changes. In order to investigate the relationship between the coseismic stress change and the aftershock distribution, we calculated ΔCFF acting on the aftershock fault planes. We used the slip distribution by Iwata and Sekiguchi (2002), which is shown in Fig. 2b. (Only the large-slip area in which slips were larger than a half of the maximum, 2 m, is shown.) We used only aftershocks for which focal mechanisms were determined. We focused on the aftershocks around Faults 1 and 2 because of the simplicity of the geometry of the mainshock fault plane. Since the focal mechanisms of only 4% of the relocated aftershocks around Faults 1 and 2 could not be determined, neglecting these events does not significantly affect the results. Stress changes due to the mainshock slip were calculated using the formula of Okada (1992). We set the rigidity to 30 GPa and the apparent coefficient of friction to 0.4. We calculated ΔCFF for both nodal planes of the focal mechanism using the stress change at its hypocenter and selected a larger value of ΔCFF.

Figure 10 shows the spatial distribution of ΔCFF for the focal mechanisms of aftershocks around Faults 1 and 2. Except in and around the large-slip region ($-10 < Y < -3.5$ km in Fig. 10b), most of the aftershocks have a positive value of ΔCFF. If we define the percentage of aftershocks having positive ΔCFF to all relocated aftershocks in a target region as the Coulomb index, the Coulomb indices around Fault 2 ($Y \geq -3.5$ km in Fig. 10b) and around the southern edge of Fault 1 ($Y \leq -10$ km) are 81 and 89%, respectively. We evaluated the statistical significance for the Coulomb indices using the bootstrap method proposed in Kato (2006). We generated a synthetic catalog that was created as a random combination of the hypocenter and focal mechanism data around Faults 1 and 2. We calculated the Coulomb index for the synthetic catalog and performed the procedure 1000 times. As a result, the Coulomb indices for 3.3 and 0.2% of the synthesized catalog around Fault 2 and around

(See figure on next page.)

Fig. 8 Characteristics of the focal mechanisms around the mainshock fault. **a** Relationship between the hypocenter distance from Fault 1 or 2 and the Kagan angle from the reference focal mechanisms. **b** Rose diagram showing the strike of nodal planes for the focal mechanisms of strike-slip type, the plunges of the P- and T-axes of which are less than or equal to 30°. We selected the nodal plane for which the strike is closer to that of the best-fit plane. The *thick black line* indicates the strike of the best-fit plane. **c** Spatial distribution of the nodal plane strike closer to that of Fault 1 or 2. The *red* and *gray lines* indicate nodal planes of strike-slip type and other types, respectively. Note that the *vertical* and *horizontal axes*, respectively, indicate the directions along and normal to the best-fit plane

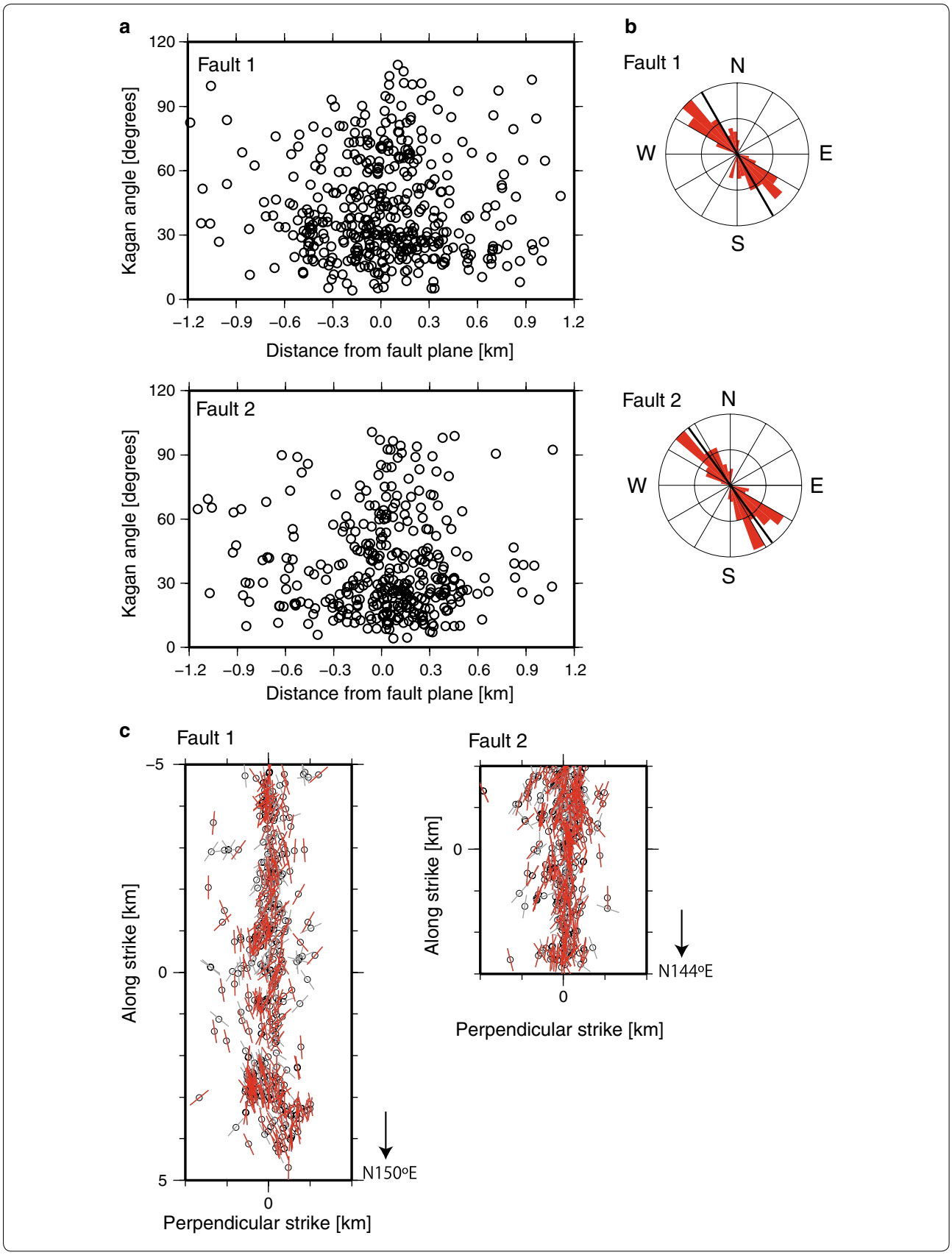
a
Fault 1
Kagan angle [degrees]
120
90
60
30
0
−1.2 −0.9 −0.6 −0.3 0.0 0.3 0.6 0.9 1.2
Distance from fault plane [km]
Fault 2
Kagan angle [degrees]
Distance from fault plane [km]
b
Fault 1
N
W
E
S
Fault 2
N
W
E
S
c
Fault 1
−5
0
5
Along strike [km]
0
Perpendicular strike [km]
N150°E
Fault 2
Along strike [km]
0
0
Perpendicular strike [km]
N144°E

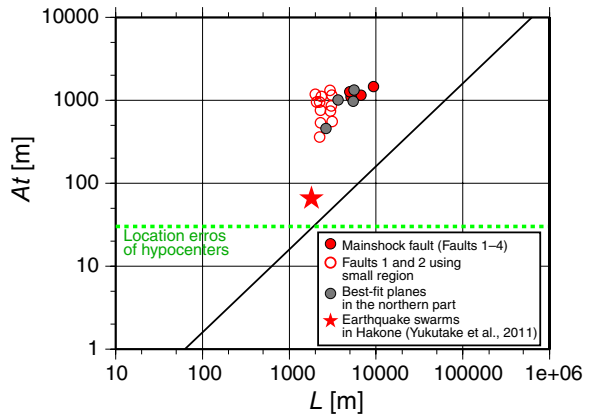

Fig. 9 Relationship between L and A_t. The *straight line* indicates the scaling between P and L based on a natural fault zone in the outcrop compiled by Vermilye and Scholz (1998). The *solid red* and *gray circles* indicate A_t around the mainshock fault (Faults 1 through 4) and the best-fit planes in the northern part of the aftershock region (Faults 5 through 8), respectively. The *red open circles* indicate A_t obtained using a smaller region for event selection around Faults 1 and 2. The *green broken line* indicates the upper limit of the location errors of hypocenters in the horizontal direction. The *red star* indicates the thickness of the hypocenter distribution and its fault length associated with the swarm activity in the volcanic area (Yukutake et al. 2011)

the southern edge of Fault 1, respectively, are equal to or greater than the Coulomb indices for the actual catalog. This implies that the triggering of aftershocks due to the static stress change is statistically significant at the 95% confidence level in these regions. This result also suggests that A_t may be controlled by the spatial distribution of stress changes. On the other hand, aftershocks having a negative value of ΔCFF were concentrated in and around the large-slip region ($-10 < Y < -3.5$ km in Fig. 10b). The Coulomb index in this region is 47%. This result implies that the true slip distribution in the large-slip region was complicated beyond the limitation of the spatial resolution of the waveform inversion or some other factor was related to the triggering of aftershocks in the large-slip region.

Difference in hypocenter distribution between an aftershock and an earthquake swarm

The red star in Fig. 9 indicates the relationship between the thickness of the hypocenter distribution and its length associated with the swarm activity in the geothermal region at Hakone volcano in central Japan (Yukutake et al. 2011). Yukutake et al. demonstrated that the hypocenters of the swarm activity were concentrated on a planar zone having a thickness comparable to the damage zone of the natural fault reported by Vermilye and Scholz (1998) and interpreted the earthquake swarms as being triggered by the migration of highly pressurized fluid within the fault damage zone, which is considered to be highly permeable and to serve as a conduit for fluid flow (e.g., Faulkner et al. 2010). Narrow zones of hypocenter distribution are also reported in the water injection-induced seismicity (e.g., Deichmann and Giardini 2009; Rutledge et al. 2004). On the other hand, the aftershocks on a fault with the same length were distributed within a significantly broader zone (Fig. 9). This result likely reflects the difference in the generation process: Aftershocks are generated primarily by the stress disturbance that acts within a widespread area, whereas earthquake swarms in the geothermal region are caused by the migration of crustal/magmatic fluid into the localized permeable zone.

Conclusions

In the present study, based on the precisely determined hypocenters and focal mechanisms, we considered the important question of why aftershocks occur. In order to address this question, we investigated whether aftershocks represent the rerupture of the mainshock fault plane or aftershocks occur on faults outside the mainshock fault plane. The aftershocks of the 2000 Western Tottori Earthquake were distributed within the zones of 1.0–1.5 km in thicknesses along the mainshock fault on which the coseismic slip occurred. These thicknesses of the aftershock zones cannot be explained by the location errors of hypocenters or the geometrical heterogeneity of the mainshock fault plane. This result suggests that most of the aftershocks represent the rupture of fractures surrounding the mainshock fault, rather than the rerupture of the mainshock fault. Moreover, the aftershocks were distributed within a much broader zone than the fault damage zone obtained in the geological observation. Since most aftershocks except in and around the large-slip region have a positive value of ΔCFF, it is suggested that the thickness of the aftershock distribution may be controlled by the stress changes caused by the slip during the mainshock. The hypocenters of the swarm activity in the geothermal region exhibit a narrower planar distribution compared with the aftershock sequence. This result implies a difference in the generation process: Earthquake swarms are controlled by the fault weakening process due to fluid intrusion into a fault damage zone that serves as a highly permeable channel, whereas aftershocks are caused primarily by stress changes due to slip dislocation during the mainshock or its afterslip. In summary, we conclude that the major factor in generating the aftershocks in this region is the stress changes caused by the slip related to the mainshock.

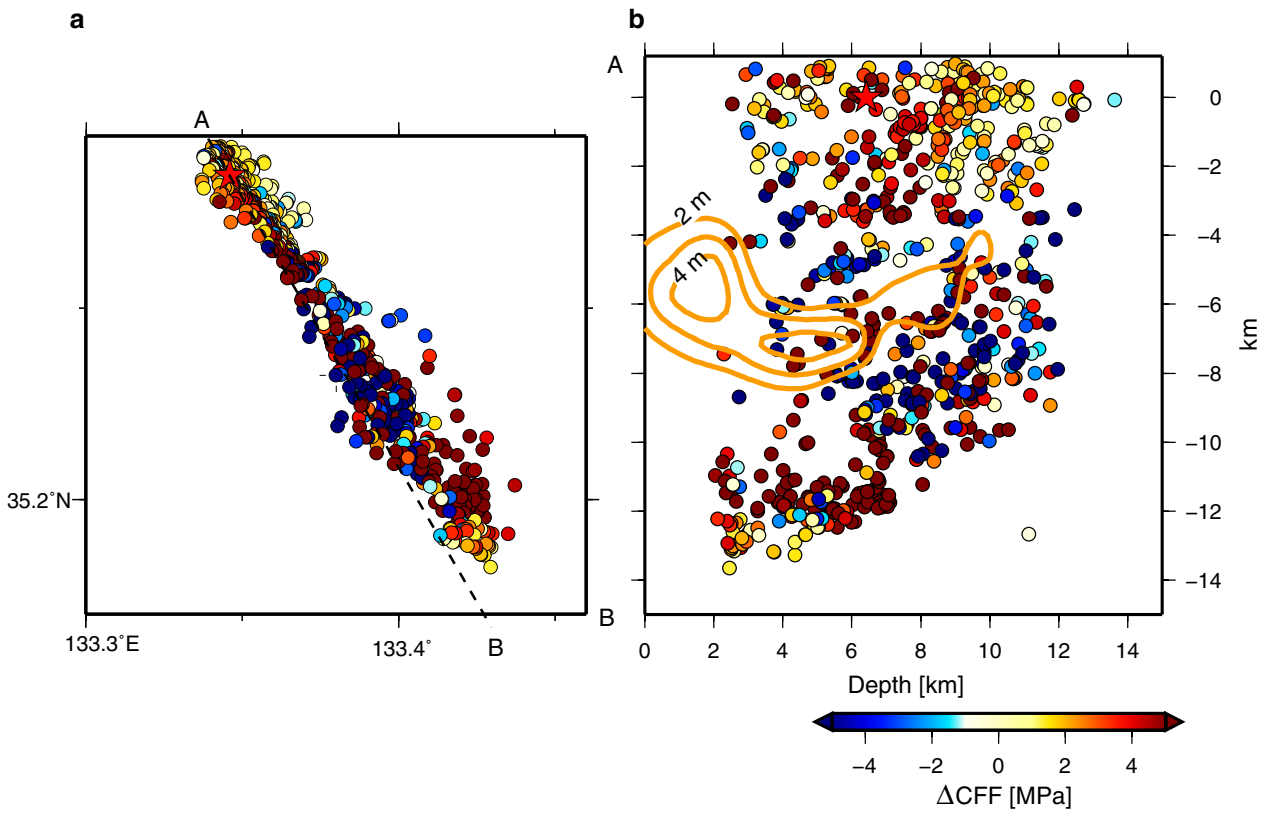

Fig. 10 Spatial distribution of ΔCFF for the aftershock focal mechanisms around Faults 1 and 2. **a** Epicentral distribution and **b** depth section on *line A–B*. The *orange* contours projected on (**b**) indicate areas of large slip exceeding a dislocation of 2.0 m as estimated by Iwata and Sekiguchi (2002). The *red star* indicates the starting point of mainshock rupture

Additional files

Additional file 1. Procedure of event selection for principal component analysis (PCA). This file describes our procedure for event selection.

Additional file 2. Validation of the thickness of aftershock distribution by using the observed differential arrival times. This file shows the waveform records to validate the thickness of aftershock distribution.

Abbreviations

DD: double difference; PCA: principal component analysis; CMT: centroid moment tensor; GNSS: global navigation satellite system; A_t: thickness of aftershock distribution; L: length of fault; P: thickness of damage zone.

Authors' contributions

YY analyzed the data and wrote the manuscript. YI assisted with the interpretation. Both authors read and approved the final manuscript.

Author details

[1] Hot Springs Research Institute of Kanagawa Prefectural Government, Odawara, Japan. [2] Disaster Prevention Research Institute Kyoto University, Uji, Japan.

Acknowledgements

We used waveform data from the seismic stations of the National Research Institute for Earth Science and Disaster Prevention, Japan Meteorological Agency, Tokyo University, and Kyoto University. Assistance in selecting the arrival times was supported by Takuya Ogawa. The authors would like to thank F. Waldhauser for providing the hypoDD code. We are thankful to two anonymous reviewers, who greatly helped us improve this manuscript.

Competing interests

The authors declare that they have no competing interests.

Funding

The present study was supported by a Grant-in-Aid for Scientific Research on Innovative Areas (KAKENHI No. 26109002) from the Ministry of Education, Culture, Sports, Science and Technology (MEXT).

Publisher's Note

Received: 9 January 2017 Accepted: 2 May 2017
Published online: 15 May 2017

References

Ben-Zion Y, Peng Z, Okaya D, Seeber L, Armbruster JG, Ozer N, Michael AJ, Baris S, Aktar M (2003) A shallow fault-zone structure illuminated by trapped waves in the Karadere-Duzce branch of the North Anatolian Fault, western Turkey. Geophys J Int 152(3):699–717. doi:10.1046/j.1365-246X.2003.01870.x

Cochran ES, Li Y-G, Shearer PM, Barbot S, Fialko Y, Vidale JE (2009) Seismic and geodetic evidence for extensive, long-lived fault damage zones. Geology 37(4):315–318. doi:10.1130/g25306a.1

Das S, Henry C (2003) Spatial relation between main earthquake slip and its aftershock distribution. Rev Geophys. doi:10.1029/2002RG000119

Deichmann N, Giardini D (2009) Earthquakes induced by the stimulation of an enhanced geothermal system below Basel (Switzerland). Seismol Res Lett 80(5):784–798. doi:10.1785/gssrl.80.5.784

Faulkner DR, Jackson CAL, Lunn RJ, Schlische RW, Shipton ZK, Wibberley CAJ, Withjack MO (2010) A review of recent developments concerning the structure, mechanics and fluid flow properties of fault zones. J Struct Geol 32(11):1557–1575. doi:10.1016/j.jsg.2010.06.009

Frohlich C (2001) Display and quantitative assessment of distributions of earthquake focal mechanisms. Geophys J Int 144(2):300–308. doi:10.1046/j.1365-246x.2001.00341.x

Fukuyama E, Ellsworth WL, Waldhauser F, Kubo A (2003) Detailed fault structure of the 2000 Western Tottori, Japan, Earthquake Sequence. Bull Seismol Soc Am 93(4):1468–1478. doi:10.1785/0120020123

Hirata N, Matsu'ura M (1987) Maximum-likelihood estimation of hypocenter with origin time eliminated using nonlinear inversion technique. Phys Earth Planet Inter 47:50–61. doi:10.1016/0031-9201(87)90066-5

Ide S (2003) Apparent break in earthquake scaling due to path and site effects on deep borehole recordings. J Geophys Res. doi:10.1029/2001jb001617

Imanishi K, Ellsworth WL, Prejean SG (2004) Earthquake source parameters determined by the SAFOD Pilot Hole seismic array. Geophys Res Lett. doi:10.1029/2004GL019420

Imanishi K, Kuwahara Y, Takeda T, Haryu Y (2006) The seismicity, fault structures, and stress field in the seismic gap adjacent to the 2004 Mid-Niigata earthquake inferred from seismological observations. Earth Planets Space 58(7):831–841. doi:10.1186/BF03351988

Iwata T, Sekiguchi H (2002) Source model of the 2000 Tottori-Ken Seibu earthquake and near-source strong ground motion. In: Proceedings of 11th Japan earthquake engineering symposium (in Japanese with English abstract), pp 125–1285

Kagan YY (1991) 3-D rotation of double-couple earthquake sources. Geophys J Int 106(3):709–716. doi:10.1111/j.1365-246X.1991.tb06343.x

Kato A (2005) Imaging the source region of the 2004 mid-Niigata prefecture earthquake and the evolution of a seismogenic thrust-related fold. Geophys Res Lett. doi:10.1029/2005gl022366

Kato M (2006) Static Coulomb failure function and aftershocks of 1995 Kobe earthquake: a statistical test. Geophys Res Lett. doi:10.1029/2006GL026970

Kawanishi R, Iio Y, Yukutake Y, Shibutani T, Katao H (2009) Local stress concentration in the seismic belt along the Japan Sea coast inferred from precise focal mechanisms: implications for the stress accumulation process on intraplate earthquake faults. J Geophys Res. doi:10.1029/2008jb005765

Liu J, Sieh K, Hauksson E (2003) A structural interpretation of the aftershock "Cloud" of the 1992 Mw 7.3 Landers earthquake. Bull Seismol Soc Am 93(3):1333–1344. doi:10.1785/0120020060

Miller SA, Collettini C, Chiaraluce L, Cocco M, Barchi M, Kaus BJ (2004) Aftershocks driven by a high-pressure CO_2 source at depth. Nature 427(6976):724–727. doi:10.1038/nature02251

Mitchell TM, Faulkner DR (2009) The nature and origin of off-fault damage surrounding strike-slip fault zones with a wide range of displacements: a field study from the Atacama fault system, northern Chile. J Struct Geol 31(8):802–816. doi:10.1016/j.jsg.2009.05.002

Ohmi S, Watanabe K, Shibutani T, Hirano N, Nakao S (2002) The 2000 Western Tottori Earthquake—seismic activity revealed by the regional seismic networks. Earth Planets Space 54(8):819–830. doi:10.1186/bf03352075

Okada Y (1992) Internal deformation due to shear and tensile faults in a half-space. Bull Seismol Soc Am 82(2):1018–1040

Research Group for Active Faults in Japan (1991) Active faults in Japan. Japanese with English abstract rev. ed. Univ. Tokyo Press

Rutledge JT, Phillips WS, Mayerhofer MJ (2004) Faulting induced by forced fluid injection and fluid flow forced by faulting: an interpretation of hydraulic-fracture microseismicity, Carthage Cotton Valley gas field, Texas. Bull Seismol Soc Am 94(5):1817–1830. doi:10.1785/012003257

Sagiya T, Nishimura T, Hatanaka Y, Fukuyama E, Ellsworth L (2002) Crustal movement associated with the 2000 Western Tottori Earthquake and its fault models. J Geol Soc Jpn 54:523–534 **(in Japanese with English abstract)**

Shearer PM (1997) Improving local earthquake locations using the L1 norm and waveform cross correlation: application to the Whittier Narrows, California, aftershock sequence. J Geophys Res Solid Earth 102(B4):8269–8283. doi:10.1029/96JB03228

Shearer PM, Hardebeck JL, Astiz L, Richards-Dinger KB (2003) Analysis of similar event clusters in aftershocks of the 1994 Northridge, California, earthquake. J Geophys Res Solid Earth 108(B1):2035. doi:10.1029/2001JB000685

Shibutani T, Iio Y, Matsumoto S, Katao H, Matsushima T, Ohmi S, Takeuchi F, Uehira K, Ky Nishigami, Enescu B (2005a) Aftershock distribution of the 2004 Mid Niigata Prefecture Earthquake derived from a combined analysis of temporary online observations and permanent observations. Earth Planets Space 57(6):545. doi:10.1186/BF03352590

Shibutani T, H Katao, Group for the Dense Aftershock Observations of the 2000 Western Tottori Earthquake (2005b) High resolution 3-D velocity structure in the source region of the 2000 Western Tottori Earthquake in southwestern Honshu, Japan using very dense aftershock observations. Earth Planets Space 57(9):825–838. doi:10.1186/BF03351861

Ueta K, Miyakoshi K, Inoue D (2002) Left-lateral deformation of headrace tunnel associated with the 2000 Western Tottori Earthquake. J Geol Soc Jpn 54:547–556 **(in Japanese with English abstract)**

Vermilye JM, Scholz CH (1998) The process zone: a microstructural view of fault growth. J Geophys Res Solid Earth 103(B6):12223–12237. doi:10.1029/98JB00957

Waldhauser F, Ellsworth WL (2000) A double-difference earthquake location algorithm: method and application to the Northern Hayward Fault, California. Bull Seismol Soc Am 90(6):1353–1368. doi:10.1785/0120000006

Yukutake Y, Iio Y, Katao H, Shibutani T (2007) Estimation of the stress field in the region of the 2000 Western Tottori Earthquake: using numerous aftershock focal mechanisms. J Geophys Res. doi:10.1029/2005jb004250

Yukutake Y, Takeda T, Obara K (2008) Fine fault structure of a moderate earthquake in the 2007 earthquake sequence of northern Mie, Japan. Earth Planets Space 60(9):981–985. doi:10.1186/BF03352854

Yukutake Y, Ito H, Honda R, Harada M, Tanada T, Yoshida A (2011) Fluid-induced swarm earthquake sequence revealed by precisely determined hypocenters and focal mechanisms in the 2009 activity at Hakone volcano, Japan. J Geophys Res. doi:10.1029/2010jb008036